Article published online: 2021-04-01

Chalcogen Bond versus Weak Hydrogen Bond: Changing Contributions in Determining the Crystal Packing of [1,2,5]-Chalcogenadiazole-Fused Tetracyanonaphthoquinodimethanes

Yusuke Ishigaki[a]
Kota Asai[a]
Takuya Shimajiri[a]
Tomoyuki Akutagawa[b]
Takanori Fukushima[c]
Takanori Suzuki*[a]

[a] Department of Chemistry, Faculty of Science, Hokkaido University, Sapporo, Hokkaido 060-0810, Japan.
[b] Institute of Multidisciplinary Research for Advanced Materials, Tohoku University, Sendai, Miyagi 980-8577, Japan
[c] Laboratory for Chemistry and Life Science, Institute of Innovative Research, Tokyo Institute of Technology, Yokohama 226-8503, Japan
tak@sci.hokudai.ac.jp

Dedicated to Peter Bäuerle on the occasion of his 65th birthday.

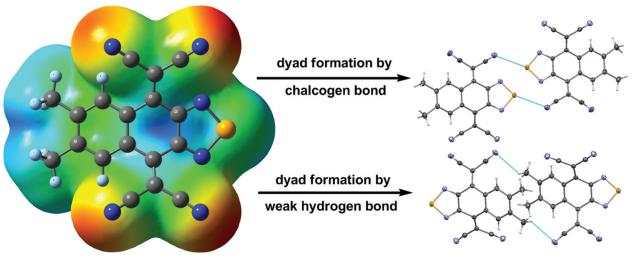

Received: 12.01.2021
Accepted after revision: 27.01.2021
DOI: 10.1055/s-0041-1725046; Art ID: om-21-0002oa

License terms:

© 2021. The Author(s). This is an open access article published by Thieme under the terms of the Creative Commons Attribution-NonDerivative-NonCommercial License, permitting copying and reproduction so long as the original work is given appropriate credit. Contents may not be used for commercial purposes, or adapted, remixed, transformed or built upon. (https://creativecommons.org/licenses/by-nc-nd/4.0/)

Abstract The crystal structures of a series of tetracyanonaphthoquinodimethanes fused with a selenadiazole or thiadiazole ring revealed that their molecular packing is determined mainly by two intermolecular interactions: chalcogen bond (ChB) and weak hydrogen bond (WHB). ChB between Se and a cyano group dictates the packing of selenadiazole derivatives, whereas the S-based ChB is much weaker and competes with WHB in thiadiazole analogues. This difference can be explained by different electrostatic potentials as revealed by density functional theory calculations. A proper molecular design that weakens WHB can change the contribution of ChB in determining the crystal packing of thiadiazole derivatives.

Key words crystal engineering, weak hydrogen bonds, chalcogen bonds, chalcogenadiazoles, tetracyanoquinodimethanes, X-ray analysis

Introduction

The weak hydrogen bond (WHB) involving less acidic C–H groups[1] than O–H/N–H groups has been used as a supramolecular synthon in crystal engineering.[2] This approach takes advantage of intermolecular interactions to determine crystal packing and contributes to the design of new solids with desired physical and chemical properties.[3] In this regard, the chalcogen bond (ChB)[4,5] has attracted much recent attention due to the high directionality of the interaction in crystal. In ChB, an electrophilic chalcogen atom (E) is bound to a Lewis base (LB) through n(LB) → σ*(E–R) electron donation in an atomic array of LB•••E–R, where R is an electron-withdrawing group. The strength of the ChB is influenced by the nature of the E atom (Se > S), the nature of the electron-deficient R group, the LB•••E–R angle (close to linear), and the basicity of LB.[6] The directionality of the ChB was explained by the existence of a σ-hole on the E atom, which defines a positive electrostatic potential region in the direction opposite the R–E bond. [1,2,5]-Chalcogenadiazoles are versatile units (R = N, LB = N) for the generation of supramolecular synthons, such as the $(N•••E)_2$ square dimer motif.[7]

In our continuing studies on the ChB observed in tetracyanoquinodimethane (TCNQ) derivatives fused with chalcogenadiazole(s),[8] we noted that the C≡N•••E motif[9] is often found in these pure organic crystals as C≡N•••E–N contacts,[10] by which a dyad structure is generated, as shown in Scheme 1a (R = N, LB = N coming from CN). This ChB motif can be used as a reliable supramolecular synthon to make an inclusion cavity in its clathrate compounds.[11] For example, in the crystal of the title molecule with a selenadiazole ring (**1A**), the dyad is further connected into an infinite "dyad-ribbon" network by another ChB. The networks are connected to each other by WHB (Scheme 1b) to complete the overall crystal structure. In a clathrate-type molecular complex of **1A** with an electron-donating guest, the same dyad ribbons are also present, between which the inclusion cavity is formed with breaking of the original WHB and reconnection at different positions with WHB. The resulting three-dimensional cavity endows **1A** with a remarkable ability to recognize the regioisomers of the guest, thus proving the importance of ChB through the C≡N•••Se–N contact in supramolecular chemisty.[12] In contrast, despite the similar molecular geometry and electronic structure, the

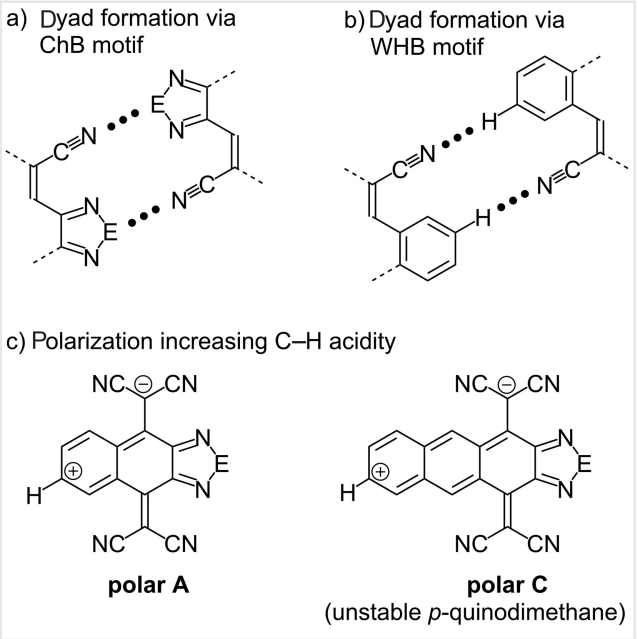

Scheme 1 Supramolecular synthons by ChB and WHB.

sulfur analogue (**2A**) does not show similar recognition properties because WHB through C≡N•••H–C contacts is a predominant factor in determining its crystal packing due to the less-effective ChB through C≡N•••S–N contacts.

Since ChB-driven molecular recognition is still considered to be in its infancy,[13] the strikingly different recognition properties between **1A** and **2A** prompted us to further study the molecular packing of other tetracyanonaphthoquinodimethane (TCNNQ) analogues fused with a chalcogenadiazole (e.g., **1B**, **1C**, **2B**, and **2C**) (Figure 1). This study sought to clarify whether a change in the chalcogen atom (Se in **1** and S in **2**) and/or proper subunit addition could alter the contribution of ChB in determining the crystal packing of the title molecules, especially in competition with WHB.

Results and Discussion

For both TCNNQs fused with a selenadiazole (**1A**) and a thiadiazole (**2A**), modification should only be done on the fused benzene ring, so that ChB would be maintained as in **1A** and **2A**. We designed here new TCNNQs by attachment of methyl groups at the 6,7-positions (**1B** and **2B**) or further annulation of a benzene ring (**1C** and **2C**) by considering that such modification affects the WHB motif shown in Scheme 1b. The carbon hybridization at C–H affects the strength of WHB: C_{sp3}–H is less effective than C_{sp2}–H.[14] Thus, WHB would have less of an influence on crystal packing in dimethyl derivative **2B** than in **2A**. The acidity of the C–H group also determines the strength of WHB,[15] and the finding that the polar C form has less of a contribution than the polar A (Scheme 1c) suggests that further annulated analogue **2C** has as less effective WHB than **2A**. These are the central points of the molecular design, and suggest that the two kinds of modification would increase the contribution of ChB in determining the crystal packing of **2** in comparison to WHB. It is highly likely that all of the crystal structures of selenadiazole derivatives (**1**) would be dictated by ChB through C≡N•••Se–N contacts, and thus the molecular packing of **1A**–**1C** can be used as a reference. Thus, a changeable contribution of ChB and WHB would be clarified when the crystal structures are compared between **1** and **2** upon weakening of the WHB through dimethylation in **2B** and further benzo-annulation in **2C**.

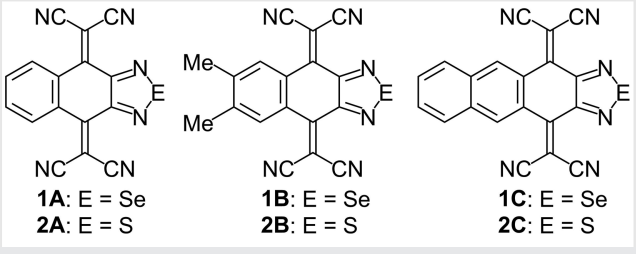

Figure 1 Dimethylation and further benzo-annulation on the TCNNQ skeleton to further weaken WHB in **1A** and **1B**.

Electrostatic potentials can provide detailed information on molecular polarization. The $V_{s,max}$ and $V_{s,min}$ values are useful for evaluating of the intermolecular interactions such as ChB and WHB. Density functional theory (DFT) calculations were conducted for **1B**, **1C**, **2B**, and **2C** [M06-2X/6-31G(d,p)] (Figure S1) and the results were compared to those of **1A** and **2A** calculated using the same function and basis set.[12] The 6-31G(d,p) basis set with a reasonable calculation cost would be satisfactory since the results were compared only among **1A**–**1C** and **2A**–**2C**, which have similar geometrical and electronic structures.

As shown in Figure 2, the electrostatic potentials of the present TCNNQs are similar to each other: large positive values on the E atom corresponding to the presence of σ-holes and on the C–H groups, and large negative values on the N atoms of cyano groups and those of chalcogenadiazoles. The $V_{s,max}$ values on Se in **1B** and **1C** (+33.3 and 33.6 kcal mol^{-1}, respectively) are similar to that in **1A** (+35.0 kcal mol^{-1}). On the other hand, $V_{s,max}$ values of the C–H groups at the opposite region on the long molecular axis in **1B** and **1C** (+25.2 and 27.1 kcal mol^{-1}, respectively) are smaller than those of **1A** (+30.5 kcal mol^{-1}) and the parent TCNNQ without a fused heterocycle (+29.9 kcal mol^{-1}). Thus, ChB should be the predominant intermolecular interaction in **1B** and **1C** with an even weaker WHB than in **1A**.

Thiadiazole compounds **2A**–**2C** have smaller $V_{s,max}$ values (+28.7, 27.0, and 27.2 kcal mol^{-1}, respectively) on S than on Se in **1A**–**1C**, and thus the $V_{s,max}$ value of the C–H groups in **2A** (+31.2 kcal mol^{-1}) is larger than them. However, when two methyl groups are attached in **2B** (+25.9 kcal mol^{-1}) and

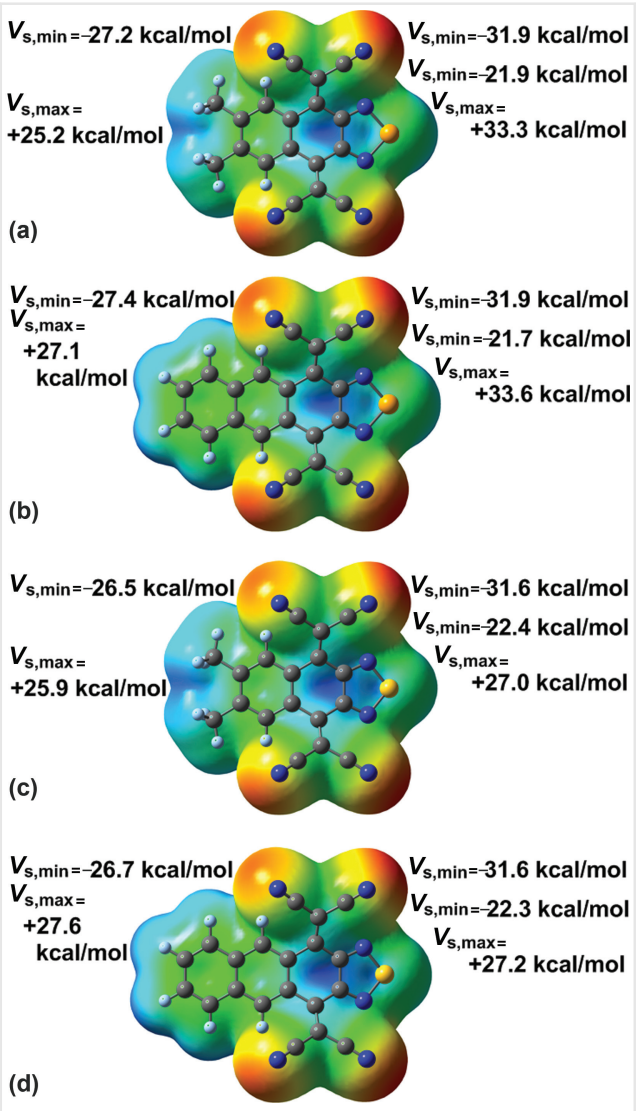

Figure 2 Electrostatic potentials in (a) **1B**, (b) **1C**, (c) **2B**, and (d) **2C** calculated by the DFT method [M06-2X/6-31G(d,p)] (isoval. = 0.0004).

further benzo-annulation is applied in **2C** (+27.6 kcal mol^{-1}), $V_{s,max}$ of the C–H groups is decreased. Thus, $V_{s,max}$ values related to ChB and WHB are comparable in **2B** and **2C**, and unlike in **2A**, both ChB and WHB should contribute to determining their crystal packing.

After the theoretical studies shown above, newly designed TCNNQs (**1B**, **1C**, **2B**, and **2C**) were prepared from the corresponding quinone derivatives[16] fused with a chalcogenadiazole ring upon condensation reactions with malononitrile in the presence of $TiCl_4$.[17] Voltammetric analyses in MeCN indicated that newly prepared TCNNQs undergo reversible electrochemical reduction (E_1^{red} and E_2^{red}/V vs. saturated calomel electrode (SCE): **1B**, –0.37 and –0.48; **1C**, –0.45 and –0.55; **2B**, –0.25 and –0.41; **2C** –0.35 and –0.41) as in other related TCNQ derivatives. The small separation between the first and second reduction potentials as in **1A** (E_1^{red} and E_2^{red}/V: –0.35 and –0.46) and **2A** (–0.22 and –0.41) indicates that these TCNNQs adopt a butterfly-shaped deformed structure,[18] which was predicted by calculation (Figure 2) and later revealed by X-ray analyses (Figures S2–S5, Table S1). Recrystallization (vapor diffusion method) from CH_2Cl_2–hexane (for **2C**) or $CHCl_3$–hexane (others) gave single crystals that were suitable for X-ray analyses as yellow plates (**1B** and **2B**) or orange plates (**1C** and **2C**).

Table 1 Geometrical description[a] for (a) ChB of C≡N•••E–N and (b) WHB of C≡N•••H–C in **1B**, **1C**, **2B**, and **2C**

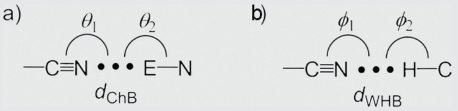

a) ChB	d_{ChB}/Å	θ1/°	θ2/°
1B (i)	3.24	123	153
1B (ii)	3.18	164	174
1C (i)	3.06	149	149
1C (ii)	3.14	139	153
2B (i)	3.44	92	130
2B (ii)	3.11	110	172
2C (i)	3.14	147	144
b) WHB	d_{WHB}/Å	φ1/°	φ2/°
1B (iii)	2.79	113	110
1B (iv)	2.79	97	122
1C (iii)	2.77	108	140
1C (iv)	2.58	164	146
2B (iii)	2.68	92	143
2B (iv)	2.89	168	179
2B (v)	2.77	152	143
2B (vi)	2.76	108	138
2C (ii)	2.82	107	139
2C (iii)	2.56	162	146

[a]The esd's for the distances and angles are less than 0.01 Å and 1°, respectively.

Selenadiazolo-TCNNQ with two methyl groups (**1B**) crystallizes in triclinic *P*-1 ($Z = 2$). The packing arrangement is mainly characterized by two kinds of ChB through C≡N•••Se–N contacts [(i) and (ii)]. The geometries of ChB can be described by the distance (d_{ChB}) of (C≡)N•••E as well as two angles (θ1: < C≡N•••E; θ2: < N•••E–N) (Table 1). By the ChB through contact (i), two molecules of **1B** form a centrosymmetric dyad, as shown in Scheme 1a. The dyad is further connected by ChB through contact (ii) along the crystallographic *b*-axis, thus forming an infinite dyad-ribbon network (Figure 3). The d_{ChB} values of (i) and (ii) are both

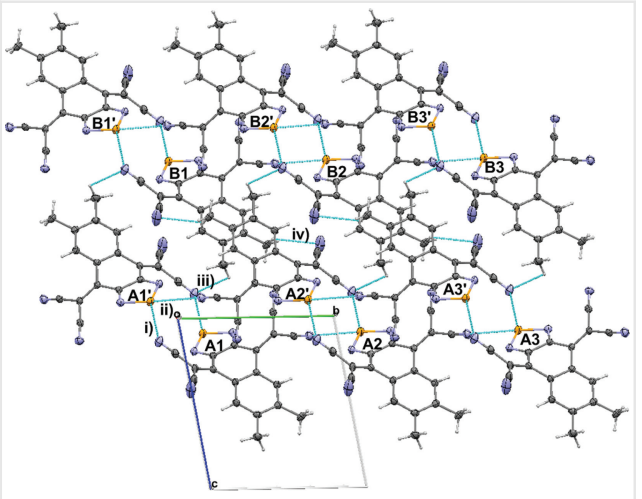

Figure 3 Sheet-like structure composed of dyad-ribbon networks in **1B**. Molecules A1 and A1' forms a dyad by ChB through contact (i). Molecules A1, A2, and A3 (as well as A1', A2', and A3') are connected by ChB through contact (ii) to form the dyad-ribbon network. Two dyad ribbons (A1-A3' and B1-B3') are connected by WHB of (iii) and (iv) between A1'and B1 and between A2' and B1, respectively.

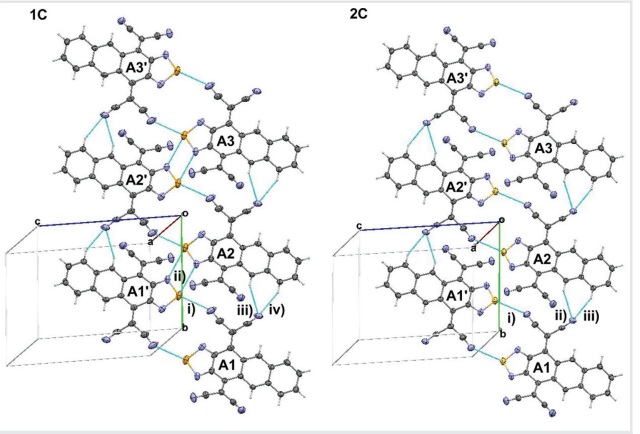

Figure 4 Dyad-ribbon network in **1C** (left) and **2C** (right). Molecules A1 and A1' forms a dyad by ChB through contact (i). Dyads are further connected along the *b*-axis to form a dyad-ribbon network (A1–A3').

smaller than the sum of the van der Waals (vdW) radii of N•••Se (3.50 Å),[19] by 7% and 9%, respectively (Table 1a). Thus, as also supported by suitable contact angles (θ1 and θ2), the ChB is proven to be a strong and important director of the crystal packing of **1B**. The positions of hydrogen atoms in **1B** were calculated geometrically, and thus there is some uncertainty regarding the parameters for WHB involving C–H of methyl groups. Despite such uncertainty, it is still clear that the dyad-ribbon networks are further connected to each other along the *c*-axis by WHB through C≡N•••H–C contacts of (iii) and (iv) (Table 1b), and thus a two-dimensional sheet-like structure is formed on the *bc*-plane. Since the sheets are repeated along the *a*-axis without significant interaction, the most characteristic feature is the sheet-like structure composed of dyad-ribbon networks. This packing is quite similar to that of **1A** (Figure S6) without methyl substitution,[12] showing that attachment of two methyl groups does not alter the packing motif because strong ChB through C≡N•••Se–N is the dominant factor in determining the crystal structure in **1A** and **1B**.

Selenadiazolo-TCNNQ with further annulation of a benzene ring (**1C**) crystallizes in triclinic *P*-1 ($Z = 2$). The packing arrangement is mainly characterized by two kinds of ChB [(i) and (ii)]. By the contact of C≡N•••Se–N (i), two molecules of **1C** form a centrosymmetric dyad, as shown in Scheme 1a. This dyad is further connected by ChB through contact (ii) of a $(N•••Se)_2$ square dimer motif to furnish the dyad-ribbon network along the crystallographic *b*-axis. The additional contacts of WHB [(iii) and (iv)] are present within the dyad ribbon (Figure 4a). In contrast to **1A** and **1B**, the dyad ribbons of **1C** are not further connected by WHB since the two C–H groups at the edge of the long molecular axis are not involved in WHB. Instead, the dyad ribbons are stacked in a layered-brick manner (Figure 5a) with two kinds of π – π overlaps (type-1: convex–convex; type-2: concave–concave) with the shortest C–C contact of 3.32 and 3.35 Å, respectively (Figure S3). Thus, the crystal packing of **1C** is governed by ChB and π – π interaction, so that the relative importance of WHB in **1C** is even less than those in **1A** and **1B**.

The crystal packing of thiadiazolo-TCNNQ with two methyl groups (**2B**) [orthorhombic, $Pca2_1$, ($Z = 4$)] is quite different from that in the corresponding selenadiazole derivative **1B**. Molecules are connected to form a sheet-like network on the *ab*-plane by WHB (iii) and (iv). There also is a

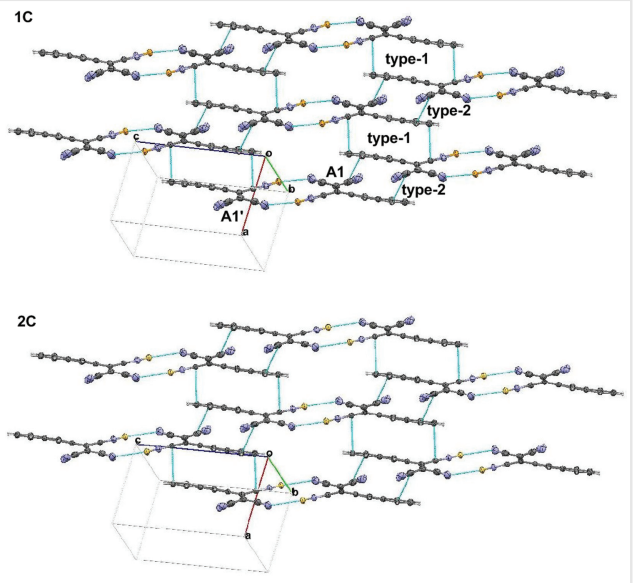

Figure 5 Layered-brick stacking of dyad-ribbon networks in **1C** (upper) and **2C** (lower) with two kinds of π–π overlaps.

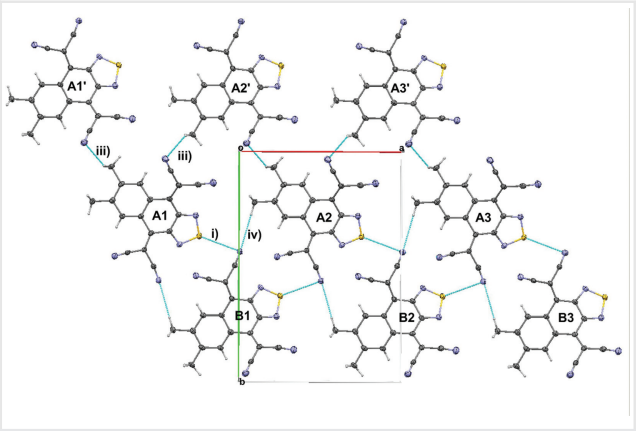

Figure 6 Sheet-like structure of **2B**. Molecule A1 is connected to A1' and A2' by WHB through contact (iii) to form a double-ribbon network (A1–A3') along the *a*-axis. This ribbon is connected to another ribbon (B1–B3) by WHB of (iv) and ChB (i) to form a sheet-like network on the *ab*-plane.

contact of C≡N•••S–N (i) with d_{ChB} of 3.44 Å, which is larger than the sum of the vdW radii of N•••S (3.35 Å)[19] and would not be considered as an effective ChB (Figure 6). Such a coplanar arrangement of molecules resembles the packing of **2A** in its molecular complex with an electron-donating guest.[12] Each molecule is further connected along the screw axis extending to the crystallographic *c*-axis. Three kinds of catemer structures are formed not only by the C≡N•••S–N contact (ii) but also by C≡N•••C–H contacts of (v) and (vi) (Figure S4). In this way, the packing arrangement of **2B** is determined by both ChB and WHB.

In contrast, thiadiazolo-TCNNQ with further annulation of a benzene ring (**2C**) [triclinic *P*-1 (Z = 2)] crystallizes isomorphous to **1C** (Figures 4b, 5b, and S5). Thus, its packing is basically determined by ChB and π – π interaction, indicating a reduced contribution from WHB due to weakening via benzo-annulation in **2C**. A notable difference is the absence of a $(N•••S)_2$ square dimer motif in **2C**, due to the generally weaker ChB in thiadiazoles than in selenadiazoles.[7a]

Conclusions

Based on the above-mentioned four X-ray structures as well as their comparisons including those of **1A** and **1B**, we can safely conclude that the contribution of ChB in thiadiazolo-TCNNQs (**2A**–**2C**) is increased by weakening WHB through two different modifications of the molecular structure. By considering that crystal packing of all the selenadiazolo-TCNNQs (**1A**–**1C**) is dictated by ChB and that **2C** has an isomorphous structure to that of **1C**, a proper molecular design (e.g., further benzo-annulation) should successfully suppress the contribution from WHB while making ChB the decisive factor for packing arrangement.

ChB through C≡N•••E–N contacts is a useful supramolecular synthon in crystal engineering, and thus chalcogenadiazole-fused electron acceptors can recognize the regioisomers of electron-donating guests in their crystalline molecular complexes.[11d] By following the general trend with stronger interaction for a Se-involving ChB than for a S-involving ChB, thiadiazole-fused acceptors can only provide the less reliable synthon of C≡N•••S–N.[12] However, by proper design to suppress competing interactions such as WHB, S-involving ChB can become the decisive factor of crystal packing. In this way, this work has demonstrated that the contribution of ChB in crystal engineering can be altered.

Experimental Section

^{1}H and ^{13}C NMR spectra were recorded on a BRUKER Ascend™ 400 (^{1}H/400 MHz and ^{13}C/100 MHz) spectrometer. IR spectra were measured on a Shimadzu IRAffinity-1S FT/IR spectrophotometer in ATR mode. UV/Vis spectra were recorded on a Hitachi U-2910 spectrophotometer. Mass spectra were recorded on a JMS-T100GCV spectrometer in FD mode by Dr. Eri Fukushi and Mr. Yusuke Takata (GC-MS & NMR Laboratory, Research Faculty of Agriculture, Hokkaido University). Melting points were measured on a Yamato MP-21 and are uncorrected.

Calculation

DFT calculations were performed with the Gaussian 16W program package. The geometries of the compounds were optimized by using the M06-2X method in combination with the 6-31G(d,p) basis set. The coordinates are given in the Supporting Information.

Synthetic Procedures

A typical procedure for conversion of the precursor quinones to TCNQs is as follows: to a suspension of 6,7-dimethylnaphtho[2,3-*c*][1,2,5]selenadiazole-4,9-dione (2.53 g, 8.69 mmol) in dry CH_2Cl_2 (200 mL) was added $TiCl_4$ (4.67 g, 24.6 mmol). To the mixture was then added dropwise a solution of malononitrile (8.11 g, 123 mmol) in a mixed solvent of dry pyridine (20 mL) and dry CH_2Cl_2 (100 mL) over 80 min. After the mixture was stirred for 45 h at 25 °C, it was poured into 4N HCl aq (400 mL). The organic layer was separated and washed with water (350 mL × 5) and brine (300 mL × 3), and then dried over Na_2SO_4. Solvent was removed and the residue was chromatographed on silica gel (CH_2Cl_2) to give **1B** as a yellow solid (3.34 g) in 99% yield. Similarly, **1C** (orange crystal), **2B** (yellow crystal), and **2C** (orange crystal) were

obtained in respective yields of 87% (224 mg), 74% (53 mg), and 82% (50 mg).

The selected spectral data for **1B**, **1C**, **2B,** and **2C** are as follows. The spectral charts are given in the Supporting Information.

1B: Mp 272–280 °C (dec); ^{1}H NMR (400 MHz, $CDCl_3$) δ = 8.31 (2 H, s), 2.49 (6 H, s), ^{13}C NMR (100 MHz, $CDCl_3$) δ = 155.22, 152.24, 144.89, 130.59, 126.79, 113.35, 112.68, 84.07, 20.45; IR (ATR): 3155, 2957, 2226, 1602, 1554, 1441, 1402, 1284, 895, 751, 573, 480, 427 cm^{-1}; HRMS-FD: *m*/*z* $[M]^+$ calcd for $C_{18}H_8N_6Se$: 387.99764; found: 387.99670; UV/Vis (CH_2Cl_2): λ_{max} (log ε) = 364sh (4.47), 336 (4.58), 266sh (3.85), 252 (3.94), 230 (4.06) nm.

1C: Mp > 400 °C; ^{1}H NMR (400 MHz, $CDCl_3$) δ = 9.03 (2 H, s), 8.11 (2 H, dd, J = 6.2, 3.2 Hz), 7.85 (2 H, dd, J = 6.2, 3.2 Hz), (400 MHz, DMSO-d_6) δ = 9.11 (2H, s), 8.22 (2H, dd, J = 6.0, 3.2 Hz), 7.89 (2H, dd, J = 6.0, 3.2 Hz); ^{13}C NMR (100 MHz, DMSO-d_6) δ = 155.47, 155.40, 133.57, 131.79, 131.43, 129.90, 125.96, 115.13, 114.21, 82.88 ; IR (ATR): 3074, 2924, 2851, 2222, 1544, 1489, 1175, 914, 901, 768, 573, 469 cm^{-1}; HRMS-FD: *m*/*z* $[M]^+$ calcd for $C_{20}H_6N_6Se$: 409.98200; found: 409.98257; UV/Vis (CH_2Cl_2): λ_{max} (log ε) = 452sh (3.80), 372 (4.43), 341 (4.72), 286sh (4.05), 258sh (4.13), 236 (4.60) nm.

2B: Mp 231–265 °C (dec); ^{1}H NMR (400 MHz, $CDCl_3$) δ = 8.42 (2H, s), 2.51 (6H, s), ^{13}C NMR (100 MHz, $CDCl_3$) δ = 152.10, 148.89, 144.96, 130.58, 126.59, 113.36, 112.38, 83.57, 20.43; IR (ATR): 3054, 2925, 2851, 2229, 1604, 1554, 1409, 1273, 975, 837, 734, 577, 525, 423 cm^{-1}; HRMS-FD: *m*/*z* $[M]^+$ calcd for $C_{18}H_8N_6S$: 340.05311; found: 340.05441; UV/Vis (CH_2Cl_2): λ_{max} (log ε) = 356 (4.46), 318 (4.49), 252sh (3.97), 230 (4.20) nm.

2C: Mp 361–362 °C; ^{1}H NMR (400 MHz, $CDCl_3$) δ = 9.13 (2H, s), 8.13 (2H, dd, J = 6.1, 3.3 Hz), 7.57 (2H, dd, J = 6.1, 3.3 Hz); ^{13}C NMR could not be measured due to low solubility; Anal. calcd for $C_{20}H_6N_6S$: C, 66.28; H, 1.67; N, 23.20%. Found: C, 66.49; H. 1.89; N. 23.15%; IR (ATR): 3076, 2925, 2853, 2223, 1590, 1543, 1487, 1443, 1249, 974, 914, 902, 845, 771, 580, 523, 470 cm^{-1}; HRMS-FD: *m*/*z* $[M]^+$ calcd for $C_{20}H_6N_6S$: 362.03746; found: 362.03814; UV/Vis (CH_2Cl_2): λ_{max} (log ε) = 453sh (3.78), 350 (4.39), 324 (4.53), 270 (4.15), 232 (4.52) nm.

Redox Potential Measurement

Cyclic voltammetric analyses were conducted on a BAS ALS-600A electrochemical analyzer in dry MeCN containing 0.1 M Et_4NClO_4 as a supporting electrolyte. All of the values shown in the text are in *E*/V vs. SCE measured at the scan rate of 100 mV s^{-1}. Pt disk electrodes were used as the working and counter electrodes. All of the waves are reversible and the E^{red} value was obtained as $(E^{cathodic\ peak} + E^{anodic\ peak})/2$. Under the similar conditions, the potential for Fe/Fc^+ is +0.38 V.

X-Ray Analyses

1B: *MF* $C_{18}H_8N_6Se$, *FW* 387.26, triclinic *P*-1, *a* = 8.7829 (2) Å, *b* = 9.6682(2) Å, *c* = 10.5357(2) Å, α = 74.1400(19)°, β = 71.387(2)°, γ = 68.505(2)°, *V* = 776.37(3) $Å^3$, ρ (Z = 2) = 1.657 g cm^{-3}. A total of 7569 independent reflections ($2\theta_{max}$: 151.5°) were measured at 150 K by using CuKα. The structure was solved by the direct method and the atomic coordinates were refined with anisotropic temperature factors. The positions of hydrogen atoms were calculated and included in the refinement with isotropic temperature factors. The final *R*, *wR*, and GOF values are 3.43%, 9.13%, and 1.066, respectively, for all data (CCDC 2048002).

1C: *MF* $C_{20}H_6N_6Se$, *FW* 409.27, triclinic *P*-1, *a* = 7.3955 (3) Å, *b* = 9.4496(4) Å, *c* = 12.4473(3) Å, α = 86.492(3)°, β = 78.650(3)°, γ = 71.114(3)°, *V* = 806.95(5) $Å^3$, ρ (Z = 2) = 1.684 g cm^{-3}. A total of 7907 independent reflections ($2\theta_{max}$: 152.7°) were measured at 150 K by using CuKα. The structure was solved by the direct method and the atomic coordinates were refined with anisotropic temperature factors. The positions of hydrogen atoms were calculated and included in the refinement with isotropic temperature factors. The final *R*, *wR*, and GOF values are 4.66%, 11.53%, and 1.047, respectively, for all data (CCDC 2048003).

2B: *MF* $C_{18}H_8N_6S$, *FW* 340.36, orthorhombic, *Pca2*$_1$, *a* = 12.18316(19) Å, *b* = 17.2162(3) Å, *c* = 7.28933(12) Å, *V* = 1528.92(4) $Å^3$, ρ(Z = 4) = 1.479 g cm^{-3}. A total of 4735 independent reflections ($2\theta_{max}$: 151.6°) were measured at 150 K by using CuKα. The structure was solved by the direct method and the atomic coordinates were refined with anisotropic temperature factors. The positions of hydrogen atoms were calculated and included in the refinement with isotropic temperature factors. The final *R*, *wR*, and GOF values are 5.54%, 14.88%, and 1.203, respectively, for all data (CCDC 2048004).

2C: *MF* $C_{20}H_6N_6S$, *FW* 362.37, triclinic *P*-1, *a* = 7.3004(5) Å, *b* = 9.4855(6) Å, *c* = 12.3573(6) Å, α = 86.461(4)°, β = 78.239(5)°, γ = 71.110(6)°, *V* = 792.62(9) $Å^3$, ρ (Z = 2) = 1.518 g cm^{-3}. A total of 7603 independent reflections ($2\theta_{max}$: 151.6°) were measured at 150 K by using CuKα. The structure was solved by the direct method and the atomic coordinates were refined with anisotropic temperature factors. The positions of hydrogen atoms were calculated and included in the refinement with isotropic temperature factors. The final *R*, *wR*, and GOF values are 5.20%, 15.12%, and 1.109, respectively, for all data (CCDC 2048005).

Funding Information

We thank the Japan Society for the Promotion of Science Kakenhi (Nos. 19K15528, 20H02719, 20K21184). Financial supports from the Hattori Hokokai Foundation, Toyota Riken Scholar, the NOVARTIS Foundation (Japan) for the Promotion of Science, and the Orange Foundation for Hepatitis B Suit Hokkaido are gratefully acknowledged.

Acknowledgment

This work was also supported by the Research Program of "Five-star Alliance" in "NJRC Mater. & Dev." MEXT.

Supporting Information

Following data are given in the Supporting Information: details of DFT calculations of **1B**, **1C**, **2B**, and **2C**; supplementary figures and table of X-ray analyses of **1B**, **1C**, **2B**, and **2C**; spectral charts for **1B**, **1C**, **2B**, and **2C**. Supporting Information for this article is available online at https://doi.org/10.1055/s-0041-1725046.

References

(1) For pioneering reviews:. (a) Desiraju, G. R. *Acc. Chem. Res.* **1991**, *24*, 290. (b) Desiraju, G. R. *Acc. Chem. Res.* **1996**, *29*, 441. (c) Desiraju, G. R. *Chem. Commun.* **2005**, 2995.

(2) (a) Huynh, H.-T.; Jeannin, O.; Fourmigué, M. *Chem. Commun.* **2017**, *53*, 8467. (b) Zhang, Y.; Wang, W. *Crystals* **2018**, *8*, 163. (c) Scilabra, P.; Terraneo, G.; Resnati, G. *Acc. Chem. Res.* **2019**, *52*, 1313.

(3) (a) Desiraju, G. R. *Angew. Chem. Int. Ed. Engl.* **1995**, *34*, 2311. (b) Nangia, A.; Desiraju, G. R. *Acta Crystallogr.* **1998**, *A54*, 934. (c) Metrangolo, P.; Neukirch, H.; Pilati, T.; Resnati, G. *Acc. Chem. Res.* **2005**, *38*, 386. (d) Desiraju, G. R. *J. Am. Chem. Soc.* **2013**, *135*, 9952.

(4) For recent reviews: (a) Lim, J. Y. C.; Beer, P. D. *Chem* **2018**, *4*, 731. (b) Vogel, L.; Wonner, P.; Huber, S. M. *Angew. Chem. Int. Ed.* **2019**, *58*, 1880. (c) Kolb, S.; Oliver, G. A.; Werz, D. B. *Angew. Chem. Int. Ed.* **2020**, *59*, 22306. (d) Ho, P. C.; Wang, J. Z.; Meloni, F.; Vargas-Baca, I. *Coord. Chem. Rev.* **2020**, *422*, 213464.

(5) For early studies: (a) Werz, D. B.; Gleiter, R.; Rominger, F. *J. Am. Chem. Soc.* **2002**, *124*, 10638. (b) Werz, D. B.; Staeb, T. H.; Benisch, C.; Rausch, B. J.; Rominger, F.; Gleiter, R. *Org. Lett.* **2002**, *4*, 339. (c) Werz, D. B.; Gleiter, R.; Rominger, F. *J. Org. Chem.* **2002**, *67*, 4290. (d) Werz, D. B.; Gleiter, R.; Rominger, F. *J. Org. Chem.* **2004**, *69*, 2945. (e) Cozzolino, A. F.; Vargas-Baca, I.; Mansour, S.; Mahmoudkhani, A. H. *J. Am. Chem. Soc.* **2005**, *127*, 3184. (f) Cozzolino, A. F.; Vargas-Baca, I. *J. Organomet. Chem.* **2007**, *692*, 2654.

(6) (a) Wang, W.; Ji, B.; Zhang, Y. *J. Phys. Chem. A* **2009**, *113*, 8132. (b) Bauzá, A.; Quiñonero, D.; Deyà, P. M.; Frontera, A. *CrystEngComm* **2013**, *15*, 3137. (c) Pascoe, D. J.; Ling, K. B.; Cockroft, S. L. *J. Am. Chem. Soc.* **2017**, *139*, 15160. (d) Sánchez-Sanz, G.; Trujillo, C. *J. Phys. Chem. A* **2018**, *122*, 1369.

(7) (a) Tsuzuki, S.; Sato, N. *J. Phys. Chem. B* **2013**, *117*, 6849. (b) Lonchakov, A. V.; Rakitin, O. A.; Gritsan, N. P.; Zibarev, A. V. *Molecules* **2013**, *18*, 9850. (c) Langis-Barsetti, S.; Maris, T.; Wuest, J. D. *J. Org. Chem.* **2017**, *82*, 5034. (d) Riwar, L.-J.; Trapp, N.; Root, K.; Zenobi, R.; Diederich, F. *Angew. Chem. Int. Ed.* **2018**, *57*, 17259. (e) Ams, M. R.; Trapp, N.; Schwab, A.; Milić, J. V.; Diederich, F. *Chem. Eur. J.* **2019**, *25*, 323.

(8) (a) Yamashita, Y.; Suzuki, T.; Mukai, T.; Saito, G. J. *Chem. Soc., Chem. Commun.* **1985**, 1044. (b) Suzuki, T.; Yamashita, Y.; Kabuto, C.; Miyashi, T. *J. Chem. Soc., Chem. Commun.* **1989**, 1102.

(9) (a) Klapötke, T. M.; Krumm, B.; Gálvez-Ruiz, J. C.; Nöth, H.; Schwab, I. *Eur. J. Inorg. Chem.* **2004**, 4764. (b) Klapötke, T. M.; Krumm, B. *Inorg. Chem.* **2008**, *47*, 7025. (c) Berrueta Martínez, Y.; Rodríguez Pirani, L. S.; Erben, M. F.; Boese, R.; Reuter, G. C. G.; Vishnevskiy, Y. V.; Mitzel, N. W.; Della Védova, C. O. *ChemPhysChem* **2016**, *17*, 1463. (d) Berrueta Martínez, Y.; Rodríguez Pirani, L. S.; Erben, M. F.; Boese, R.; Reuter, C. G.; Vishnevskiy, Y. V.; Mitzel, N. W.; Della Védova, C. O. J. *Mol. Struct.* **2017**, *1132*, 175. (e) Previtali, V.; Sánchez-Sanz, G.; Trujillo, C. *ChemPhysChem* **2019**, *20*, 3186.

(10) (a) Kabuto, C.; Suzuki, T.; Yamashita, Y.; Mukai, T. *Chem. Lett.* **1986**, *15*, 1433. (b) Suzuki, T.; Kabuto, C.; Yamashita, Y.; Saito, G.; Mukai, T.; Miyashi, T. *Chem. Lett.* **1987**, *16*, 2285. (c) Suzuki, T.; Yamashita, Y.; Fukushima, T.; Miyashi, T. *Mol. Cryst. Liq. Cryst.* **1997**, *296*, 165.

(11) (a) Suzuki, T.; Kabuto, C.; Yamashita, Y.; Mukai, T.; Miyashi, T.; Saito, G. *Bull. Chem. Soc. Jpn.* **1987**, *60*, 2111. (b) Suzuki, T.; Kabuto, C.; Yamashita, Y.; Mukai, T.; Miyashi, T.; Saito, G. *Bull. Chem. Soc. Jpn.* **1988**, *61*, 483. (c) Suzuki, T.; Kabuto, C.; Yamashita, Y.; Mukai, T.; Miyashi, T. *J. Chem. Soc., Chem. Commun.* **1988**, 895. (d) Suzuki, T.; Fujii, H.; Yamashita, Y.; Kabuto, C.; Tanaka, S.; Harasawa, M.; Mukai, T.; Miyashi, T. *J. Am. Chem. Soc.* **1992**, *114*, 3034. (e) Suzuki, T.; Fukushima, T.; Yamashita, Y.; Miyashi, T. *J. Am. Chem. Soc.* **1994**, *116*, 2793.

(12) Ishigaki, Y.; Asai, K.; Jacquot de Rouville, H.-P.; Shimajiri, T.; Heitz, V.; Fujii-Shinomiya, H.; Suzuki, T. *Eur. J. Org. Chem.* **2021**, 990.

(13) Biot, N.; Bonafazi, D. *Coord. Chem. Rev.* **2020**, *413*, 213243.

(14) (a) Vishveshwara, S. *Chem. Phys. Lett.* **1978**, *59*, 26. (b) Sreerama, N.; Vishveshwara, S. *J. Mol. Struct. THEOCHEM* **1985**, *133*, 139. (c) Domagała, M.; Grabowski, S. J. *J. Phys. Chem. A* **2005**, *109*, 5683.

(15) (a) Dejiraju, G. R. *J. Chem. Soc., Chem. Commun.* **1989**, 179. (b) Pedireddi, V. R.; Desiraju, G. R. *J. Chem. Soc., Chem. Commun.* **1992**, 988.

(16) (a) Akasaki, Y.; Aonuma, H.; Kongo, K.; Sato, K.; Nukada, K.; Marumo, A. *Jpn. Kokai Tokkyo Koho* **1990**, JP02097963A 19900410. (b) Yamashita, Y.; Tanaka, S.; Imaeda, K. *Synth. Met.* **1995**, *71*, 1965. (c) Shi, S.; Katz, T. J.; Yang, B. V.; Liu, L. *J. Org. Chem.* **1995**, *60*, 1285.

(17) (a) Lehnert, W. *Tetrahedron Lett.* **1970**, *11*, 4723. (b) Aumüller, A.; Hünig, S. *Liebigs Ann. Chem.* **1984**, 618.

(18) (a) Schubert, U.; Hünig, S.; Aumüller, A. *Liebigs Ann. Chem.* **1985**, 1216. (b) Martin, N.; Hanack, M. *J. Chem. Soc., Chem. Commun.* **1988**, 1522. (c) Gómez, R.; Seoane, C.; Segura, J. L. *Chem. Soc. Rev.* **2007**, *36*, 1305. (d) Bureš, F.; Bernd Schweizer, W.; Boudon, C.; Gisselbrecht, J.-P.; Gross, M.; Diederich, F. *Eur. J. Org. Chem.* **2008**, 994. (e) Ishigaki, Y.; Sugawara, K.; Yoshida, M.; Kato, M.; Suzuki, T. *Bull. Chem. Soc. Jpn.* **2019**, *92*, 1211. (f) Ishigaki, Y.; Hayashi, Y.; Suzuki, T. *J. Am. Chem. Soc.* **2019**, *141*, 18293. (g) Ishigaki, Y.; Hashimoto, T.; Sugawara, K.; Suzuki, S.; Suzuki, T. *Angew. Chem. Int. Ed.* **2020**, *59*, 6581.

(19) Pauling, L. The nature of the chemical bond and the structure of molecules and crystals: An introduction to modern structural chemistry. 3rd ed; Cornell University Press: Ithaka, NY, **1960**.